Ecotoxicology and Environmental Safety 257 (2023) 114940

Contents lists available at ScienceDirect

Ecotoxicology and Environmental Safety

journal homepage: www.elsevier.com/locate/ecoenv

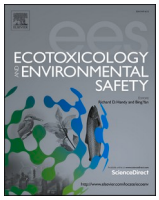

Fluoride disrupts intestinal epithelial tight junction integrity through intracellular calcium-mediated RhoA/ROCK signaling and myosin light chain kinase

Lianxin Li [a,1], Jinge Xin [a,1], Hesong Wang [b,1], Yadong Wang [c,1], Weiqi Peng [b,1], Ning Sun [a], Haonan Huang [a], Yanxi Zhou [a], Xingmei Liu [a], Yu Lin [c], Jing Fang [a], Bo Jing [a], Kangcheng Pan [a], Yan Zeng [a], Dong Zeng [a], Xiang Qin [d,*], Yang Bai [b,c,**], Xueqin Ni [a,*]

[a] Animal Microecology Institute, College of Veterinary, Sichuan Agricultural University, Chengdu, Sichuan, China
[b] Baiyun Branch, Nanfang Hospital, Southern Medical University, Guangzhou, China
[c] Guangdong Provincial Key Laboratory of Gastroenterology, Department of Gastroenterology, Institute of Gastroenterology of Guangdong Province, Nanfang Hospital, Southern Medical University, Guangzhou, China
[d] School of Life Science and Technology, University of Electronic Science and Technology of China, Chengdu, China

ARTICLE INFO

Edited by Dr. Caterina Faggio

Keywords:
Fluoride
Intestinal epithelial barrier
Tight junction
Rho kinase
Myosin light chain kinase
Intracellular calcium level

ABSTRACT

Fluoride is a common contaminant of groundwater and agricultural commodity, which poses challenges to animal and human health. A wealth of research has demonstrated its detrimental effects on intestinal mucosal integrity; however, the underlying mechanisms remain obscure. This study aimed to investigate the role of the cytoskeleton in fluoride-induced barrier dysfunction. After sodium fluoride (NaF) treatment of the cultured Caco-2 cells, both cytotoxicity and cytomorphological changes (internal vacuoles or massive ablation) were observed. NaF lowered transepithelial electrical resistance (TEER) and enhanced paracellular permeation of fluorescein isothiocyanate dextran 4 (FD-4), indicating Caco-2 monolayers hyperpermeability. In the meantime, NaF treatment altered both the expression and distribution of the tight junction protein ZO-1. Fluoride exposure increased myosin light chain II (MLC2) phosphorylation and triggered actin filament (F-actin) remodeling. While inhibition of myosin II by Blebbistatin blocked NaF-induced barrier failure and ZO-1 discontinuity, the corresponding agonist Ionomycin had effects comparable to those of fluoride, suggesting that MLC2 serves as an effector. Given the mechanisms upstream of p-MLC2 regulation, further studies demonstrated that NaF activated RhoA/ROCK signaling pathway and myosin light chain kinase (MLCK), strikingly increasing the expression of both. Pharmacological inhibitors (Rhosin, Y-27632 and ML-7) reversed NaF-induced barrier breakdown and stress fiber formation. The role of intracellular calcium ions ($[Ca^{2+}]_i$) in NaF effects on Rho/ROCK pathway and MLCK was investigated. We found that NaF elevated $[Ca^{2+}]_i$, whereas chelator BAPTA-AM attenuated increased RhoA and MLCK expression as well as ZO-1 rupture, thus, restoring barrier function. Collectively, above-mentioned results suggest that NaF induces barrier impairment via Ca^{2+}-dependent RhoA/ROCK pathway and MLCK, which in turn triggers MLC2 phosphorylation and rearrangement of ZO-1 and F-actin. These results provide potential therapeutic targets for fluoride-induced intestinal injury.

1. Introduction

Fluorine, typically in the form of fluoride, is widely distributed in the atmosphere, water, food, and soil; it is the thirteenth most abundant element. Fluoride is used to inhibit dental caries at low concentrations (Miranda et al., 2018), but excessive fluoride intake poses a serious hazard to human health (Zuo et al., 2018). It is alarming that more than 500 million people in 25 countries face the threat of high fluorine exposure, with up to 200 million at risk for fluorosis (Rafique et al., 2015). Epidemiological studies have shown that fluorine is released into

* Corresponding authors.
** Corresponding author at: Baiyun Branch, Nanfang Hospital, Southern Medical University, Guangzhou, China.
E-mail addresses: qin.xiang@foxmail.com (X. Qin), baiyang1665@smu.edu.cn (Y. Bai), xueqinni@foxmail.com (X. Ni).
[1] These authors are equal contributors.

https://doi.org/10.1016/j.ecoenv.2023.114940
Received 1 February 2023; Received in revised form 12 April 2023; Accepted 18 April 2023
Available online 24 April 2023

the environment by both geological factors or agricultural activities. Fluorine-contaminated groundwater is the primary source of fluoride exposure, causing an estimated 260 million people to suffer from endemic diseases such as skeletal fluorosis, dental fluorosis, and digestive system ailments (Jha and Tripathi, 2021). With the development of industrialization and urbanization, the scope of global fluorine pollution is expanding, particularly in some developing countries (e.g. China and India) (Rafique et al., 2015). F^- pollution is severe and common in China: a recent study showed that 70% of groundwater in the lower flood plain of Yellow River exceeds the Chinese drinking water standard of 1 mg/L (Chen et al., 2021). Similarly, chronic fluorosis has become prevalent in India, affecting more than 20 states (Choubisa and Choubisa, 2016). Excessive fluoride has been shown to have severe adverse effects on human and animal health, resulting in multiple organ failure, however, effective prevention and control methods are currently lacking. Nanocomposite materials have been widely used to remediate environmental pollutants (Mahdavi et al., 2022; Zinatloo and Zinatloo, 2019). Studies have suggested that gelatin nanoparticles are able to adsorb fluoride and reduce its exposure (Preethi et al., 2021). Safe and more sophisticated processing methods are required. Zinatloo and colleagues (Qazvini and Zinatloo, 2011; Zinatloo and Qazvini, 2014; Zinatloo and Qazvini, 2015) found that using water-soluble carbodiimide (CDI) and N-hydroxysuccinimide (NHS) as crosslinking agents ensured the stability of gelatin nanoparticles while diminishing their toxicity.

The primary route of fluoride exposure in humans is through ingestion of contaminated water or foods with high levels of fluoride accumulation, including canned meat (Fein and Cerklewski, 2001) and brick tea (Fung et al., 1999). Based on previous reports, over 60% of fluorine is absorbed in the gastrointestinal tract (Dec et al., 2017); the detrimental effects of fluoride on intestine have been extensively verified. Rat studies have shown that acute fluoride exposure caused morphological alterations in the intestine, particularly a reduction in the thickness of the tunica muscularis (Dionizio et al., 2020). Moreover, long-term high fluoride consumption resulted in severe swelling, shortening, and fusion of small intestinal villi; serum levels of D-lactic acid and diamine oxidase, biomarkers of intestinal leakage, enhanced significantly (Li et al., 2020). Murine metenteron structure is also affected by fluoride, with the proliferation of rectal epithelial cells dramatically inhibited (Wang et al., 2020). In cultured intestinal epithelial cells, fluoride resulted in cell death by elevating lipid peroxidation and glutathione depletion (Job et al., 2021). It was reported in our group that fluoride disrupts murine intestinal mucosal integrity, which is relevant to ileal tight junction (TJ) protein disruption and villous dysplasia (Sun et al., 2020; Xin et al., 2021b).

The intestinal tract, as the first barrier against foreign pollutants, includes physical, immunological, and chemical barriers. Its health is an indispensable factor for the maintenance of host homeostasis. Physical barrier, the key line of defense, is formed by epithelial cells and the TJ. TJ acts as paracellular gates that impose size- and charge-dependent restrictions on diffusion, constructed by a network of protein interactions in the apical region of the lateral membrane (Zihni et al., 2016). Existing researches have demonstrated that alterations in the continuity and/or number of tight junction proteins control epithelial permeability (Buckley and Turner, 2018). Zhang et al. (2020) reported that zearalenone damage TJs, leading to intestinal mucosal impairment in rats, in turn aggravating dysbiosis and inflammation. Jiang et al. (Jiang et al., 2021) demonstrated that exogenous basic fibroblast growth factor attenuated the breakdown of intestinal mucosal integrity after burns by upregulating TJ expression. Importantly, far from being static regions, tight junctions are directly or indirectly connected to the actin cytoskeleton; a well-studied example is zonula occludens 1 (ZO-1), which couples with F-actin via its proline-rich carboxy-terminus to serve as a critical scaffold protein (Zihni et al., 2016). When the cytoskeleton undergoes remodeling, the location of ZO-1 is changed accordingly. Zou et al. (Zou et al., 2018) reported that NF-κB-induced F-actin rearrangement engendered ZO-1 to enter the cytoplasm from cellular junctions, and this endocytosis exacerbated intestinal barrier loss. Generally, interactions with the cytoskeleton play essential roles in regulating TJ function, facilitating barrier and tissue integrity, but plastic enough to undergo remodeling when necessary (Arnold et al., 2017).

RhoA is an important small GTPase that mediates multiple critical cellular processes, including actin polymerization, proliferation and migration (Cáceres et al., 2005; Jaffe and Hall, 2005). ROCKs are the most important effectors downstream of RhoA and contribute to tension control in the apical perijunctional F-actin ring (Li et al., 2018). The Ca^{2+}-dependent kinase MLCK has been reported to modulate actomyosin organization (Cunningham and Turner, 2012). A wealth of research indicates that the activation of Rho/ROCK signaling and MLCK synergistically phosphorylates myosin light chain, which in turn promotes perijunctional actomyosin ring contraction and TJ disruption (Arnold et al., 2017; Campos et al., 2009; Cunningham and Turner, 2012). Another study showed that pro-inflammatory cytokines resulted in the phosphorylation of MLC2 via RhoA overactivation, eventually compromising TJ integrity during mucosal inflammation (Capaldo and Nusrat, 2009). Conversely, inhibition of Rho/ROCK signaling or MLCK ameliorates TJ breaking to restore barrier integrity. (Schwarz et al., 2007) Pretreatment with a MLCK inhibitor, ML-7, reversed inflammation-induced occludin endocytosis in cultured epithelia. Similarly, blocking RhoA/ROCK pathway by Fasudil and Y-27632 weakened pathogenic yeasts-triggered F-actin remodeling and ZO-1 down-regulation in Caco-2 cells (Mirza et al., 2012).

Fluoride affects cellular calcium ion homeostasis, with an enhancement in intracellular calcium levels observed in multiple model systems (Aulestia et al., 2020; Zhang et al., 2016). Fluoride inhibited calcium transporter and channel activity, promoting calcium release from intracellular stores (Matsuo et al., 2000). Xu et al. (2013) proved that high fluoride exposure leads to oxidative stress and apoptosis by elevating intracellular calcium concentrations in cultured neuroblastoma cells. Calcium ion is a highly versatile messenger in the modulation of TJs and actin filaments. It is well established that extracellular Ca^{2+} interacts with tight junctions to promote their stability (Balda et al., 1991). Cytoplasmic calcium is conducive to the assembly of TJs with cytoskeleton (Nigam et al., 1992). Additionally, calcium ions have been widely reported as mediators of cellular signaling. Ca^{2+} activates MLCK to drive actomyosin reorganization, resulting in the disconnection of tight junctions (Ducibella and Fissore, 2008). Additionally, $[Ca^{2+}]_i$ oscillations have been proved to modulate the status of the RhoA/ROCK pathway, and forestalling its overload may rescue barrier hyperpermeability caused by ethanol (Elamin et al., 2014).

Although high fluoride exposure has been shown to cause intestinal injury, the exact mechanism remains obscure. And, it is unknown whether cytoskeleton participates in fluoride-induced barrier impairment. We therefore established an in vitro model of the intestinal epithelium using Caco-2 cells and investigated the effect of NaF exposure on intestinal barrier function and its potential mechanisms. Our findings identify multiple valuable therapeutic targets for preventing and treating fluoride-induced gastrointestinal injury.

2. Methods and materials

2.1. Cell culture and treatment

Caco-2 cells, obtained from the China Center For Type Culture Collection (CCTCC, China) were grown in Dulbecco's Modified Eagle's Medium (GIBCO, USA) supplemented with 4.5 g L^{-1} glucose, 10% fetal bovine serum (PAN BIOTECH, Germany), 100 U/ML penicillin, and 100 mg/ML streptomycin (Solarbio, China), in a 5% CO_2 incubator at 37 °C. Prior to the experiment, NaF (purity>99%, Sigma Aldrich, USA) was dissolved in sterile deionized water and then diluted by DMEM. After cells grew to 80% confluence, they were exposed to different dosages of NaF for 24 h. To avoid bias, control cells were cultured without serum. The intracellular calcium chelator BAPTA-AM (15 mM, MCE, USA), the

extracellular calcium chelator EGTA (0.4 M, MCE, USA), the RhoA inhibitor Rhosin hydrochloride (40 mM, MCE, USA), the ROCK inhibitor Y27632 2HCl (40 mM, Selleck, USA), the myosin II inhibitor blebbistatin (50 mM, Abcam, UK), the agonist ionomycin (10 mM, Abcam, UK) or the MLCK inhibitor ML-7 (10 mM, Selleck, USA) was added to serum-free DMEM before 3.2 mM NaF co-incubation.

2.2. Cell viability assay

The viability of cells was assessed using Cell counting Kit-8 (CCK-8, Dojindo, Japan). Caco-2 cells were cultured in 96-well plates at a density of 0.8–1.0 $\times$ 10^5 cells/ML, with five replicates per condition. After treatment, 10% CCK-8-DMEM solution was added to 96-well plates and incubated at 37 °C with 5% CO_2 for 2 h. Optical density (OD) was measured at 450 nm using a microplate spectrophotometer (Thermo Scientific, USA).

2.3. Apoptosis assay

An Annexin V-FITC/PI Apoptosis Detection kit (BD Biosciences) was used according to the manufacturer's instructions. Caco-2 cells were seeded in 6-well plates at a density of 2 $\times$ 10^5/well. Following treatment, adherent cells were harvested, washed with PBS, and suspended in 100 μL of binding buffer. Subsequently, 5 μL of annexin V-FITC and 5 μL of propidium iodide (PI) were added, followed by incubation for 20 min at room temperature in the dark, followed by addition of another 400 μL of binding buffer and mixing. Apoptosis was measured using flow cytometry (BD FACS Canco II, USA), with early apoptosis was indicated by the percentage of cells in the Q3 quadrant and late apoptosis was indicated by the percentage of cells in the Q2 quadrant.

2.4. Monolayer integrity assays

2.4.1. TEER

Caco-2 cells were seeded at a density of 2 $\times$ 10^5 cells/well in 12-well Transwell inserts (polycarbonate membranes, 0.4 μm pore size, 0.33 cm^2 growth area; Corning Costar, USA) and incubated for 19–21 days to allow for complete cell differentiation and formation of a monolayer. The culture medium was replaced every other day during differentiation. The integrity of the cell monolayer was assessed by measuring transepithelial electrical resistance (TEER) prior to treatment using the Millicell Electrical Resistance System (Merck, Millipore, USA). Sterile cleaning was performed before insertion of the electrode. TEER values are expressed as ohm $\times$ cm^2. Caco-2 monolayers with a baseline TEER greater than 350 Ω $\times$ cm^2 were deemed to be confluent (Ebert et al., 2005).

2.4.2. Fluorescein dextran permeability

After measuring the TEER, 100 ML of 1 mg/ML FD-4 in transport buffer was added to the top chamber and 500 μL of transport buffer was poured into the bottom chamber. Transwell was incubated at 37 °C for 2 h while being shaken at 100 rpm on a microplate shaker (Thermo Scientific). The fluorescence of the lower chamber buffer (excitation at 493 and emission at 519 nm) was measured using a microplate spectrophotometer with full-wavelength reading (Thermo Scientific, USA). Monolayer permeability was calculated as the ratio of the amount of FD-4 that infiltrated into the lower chamber to the amount initially present in the upper chamber. Two independent assays were performed. A standard curve of FD-4 from 200 to 0.3125 μg/ML was constructed.

2.5. Western blotting

Caco-2 cells were washed three times with PBS, then lysed on ice in RIPA buffer. Using cell scrapers, lysates were scraped from plates and centrifuged at 10,000 $\times$ *g* at 4 °C for 10 min. Protein was quantified using a BCA Protein Assay Kit (Boster Biotechnology, China). Denatured protein samples were separated by SDS-polyacrylamide gel electrophoresis and transferred to PVDF membranes (BioRad, USA). Membranes were immersed in 5% nonfat dry milk and agitated for one hour at room temperature on a microplate shaker to decrease nonspecific binding, then incubated with primary antibody overnight at 4 °C, followed by a 1-h incubation with secondary HRP goat anti-rabbit (1:6000) antibody (Boster Biotechnology, China) at room temperature. Blots were washed thrice in TBS-Tween 0.1%, then visualized with hypersensitive ECL agents (NCM Biotech, China). We used rabbit anti-RhoA (1:5000, Abcam, UK), rabbit anti-ROCK1 and anti-ROCK2 (1:1000, Abcam, UK), rabbit anti-phospho-MLC2 (1:1000, Cell Signaling Technology, USA), rabbit anti-MLCK (1:1000, Thermo Scientific, USA), rabbit anti-ZO-1 (1:1000, Proteintech, China), and rabbit anti-GAPDH (1:3000, Affinity Biosciences, China) as primary antibodies. Band intensities were quantified using ImageJ software.

2.6. Immunofluorescence

Caco-2 cells were inoculated into confocal dishes at 1 $\times$ 10^5/ML and treated as described above. After treatment, cells were washed with PBS and fixed with 4% paraformaldehyde at room temperature for 20 min, then permeabilized for 10 min with 0.3% Triton X-100 (Solarbio, China) in PBS, then blocked for 1 h with 5% BSA (Solarbio, China) in PBS. The following primary antibodies were used overnight at 4 °C: rabbit anti-RhoA (1: 100, Abcam, UK), rabbit anti-ROCK1 and anti-ROCK2 (1: 100, Abcam, UK), rabbit anti-phospho-MLC2 (1: 100, Cell Signaling Technology, USA), rabbit anti-MLCK (1: 200, Thermo Scientific, USA), and rabbit anti-ZO-1 (1: 200, Abcam, UK). After washing, cells were treated for 3 h at room temperature with anti-rabbit secondary antibody conjugated with Alexa Fluor 488 (1: 400, Invitrogen, USA). F-actin was visualized with rhodamine-phalloidin (1:1000, AAT Bioquest, USA) and nuclei were counterstained with 4′,6-diamino-2-phenylenediamine dihydrochloride (DAPI, MCE, USA) for 15 min. Zeiss LSM 800 (Zeiss, Germany) confocal micrographs were obtained and analyzed using ImageJ software.

2.7. Detection of intracellular calcium

Cal-520 AM (AAT Bioquest, USA) was used for its high sensitivity, long wavelength, and > 100-fold fluorescence amplification, making it an ideal indicator for intracellular calcium measurement. Caco-2 cells were seeded into confocal dishes at 1 $\times$ 10^5/ML and treated as described above. After treatment, the medium was substituted with D-Hanks buffer containing 5 mM Cal-520 AM then incubated for 2 h at 37 °C. Nuclei were labeled with DAPI for 15 min. Images were captured using a Zeiss LSM 800, with 488 nm argon laser excitation and 525 nm emission. For flow cytometry, samples were washed twice in D-Hanks buffer, stained with Cal 520-AM. Fluorescence was measured using a flow cytometer at excitation wavelengths of 490 or 493 nm and emission wavelength of 525 nm. Mean fluorescence intensity was calculated using FlowJo software.

2.8. Statistical analysis

All results are presented as means ± standard deviation (SD) of at least three independent experiments. The Shapiro-Wilk test was used to analyze normality. When data were not normally distributed, they were logarithmically transformed for analysis. The Kruskal-Wallis test was performed on non-normally distributed data using the Wilcoxon rank-sum test. When data were regularly distributed, one-way analysis of variance (ANOVA) and Duncan's multiple range test were used. $P < 0.05$ was considered to indicate statistical significance. Data were analyzed using SPSS.

3. Results

3.1. NaF cytotoxic

After 24 h of NaF treatment (from 0.1 mM to 9.6 mM), the cell survival rate decreased in a dose-dependent manner from 99% to 25% of control (Fig. 1A). Concentrations equal to or below 1.6 mM did not cause significant toxicity in Caco-2 cells ($P > 0.05$), 3.2 mM NaF resulted in a noticeable decrease in cell viability ($P < 0.01$), while still exceeded 80%. Caco-2 cells were resistant to the cytotoxic effects of multiple concentrations of BAPTA-AM, EGTA, Rhosin, Y27632, Blebbistatin, Ionomycin, and ML-7 ($P > 0.05$) (Fig. S1). After 24 h of treatment, cellular morphology was analyzed (Fig. 1B). 1.6 mM NaF showed no observable morphological changes, whereas the cells subjected with 3.2 mM NaF became rounder and exhibited vacuole formation. Additionally, 6.4 mM NaF induces extensive internal cavitation and cell death. At 3.2 mM NaF, the annexin V-FITC and PI double-staining rate of apoptosis was 3.75-fold over that of the control (Fig. 1C).

3.2. NaF increased intestinal permeability and reduced ZO-1 protein

To evaluate the effect of NaF exposure on intestinal integrity, we first measured the transepithelial electrical resistance (TEER) values and cell bypass volume of fluorescent tracers using FD-4 (Fig. 2A and Fig. 2B). To monitor monolayer formation, we detected the TEER every two days. TEER in this model exceeds 400 $\Omega \times \cdot cm^2$ at seeding Day 19 (Fig. S2); after the administration of NaF for 24 h, the TEER value declined gradually with NaF dose, from 437.7 to 368.3, 127.4 and 8.58, respectively. Furthermore, the flux of the indicator FD-4 crossing into the lower chamber increased by 1.53-, 2.13- and 7.74-fold, respectively, over that of control plates. Expression of the scaffold protein ZO-1 was evaluated by western blotting; although there was no discernible change in 1.6 mM NaF-treated cells, dramatic reductions could be observed at the 3.2 mM and 6.4 mM doses (control vs. 3.2 mM NaF, $P < 0.01$; control vs. 6.4 mM NaF, $P < 0.001$) (Fig. 2C). To obviate the intervention of cell death in intestinal barrier dysfunction, 3.2 mM NaF was used as the optimal concentration in subsequent experiments. As shown in Fig. 2D, ZO-1 was uniformly distributed across the membrane surface of untreated Caco-2 cells. After 24 h of 3.2 mM NaF treatment, the intensity of ZO-1fluorescence decreased noticeably compared with the control, showing irregular cell border labeling, indicating that the intact linear structure of ZO-1 had been disrupted.

3.3. NaF increases intracellular MLC phosphorylation and regulates paracellular permeability

The phosphorylation of myosin light chain II (MLC-2) is a pivotal regulatory event in the coordination of TJs through perijunctional actomyosin ring contractions in a wide range of experimental systems (Al Nabhani et al., 2017; Su et al., 2013; Wang et al., 2018). As a biochemical marker, p-MLC2 expression was evaluated in NaF-treated cells using western blotting. Shown in Fig. 3 A, there was no obvious difference between untreated and 1.6 mM NaF-treated cells ($P = 0.2205$), whereas p-MLC2 was up-regulated remarkably in the dose of 3.2 mM and 6.4 mM (control vs. 3.2 mM NaF, $P = 0.0107$; control vs. 6.4 mM NaF, $P < 0.0001$), compared with the control. To further examine whether p-MLC2 plays an essential role in the NaF-induced reorganization of TJs and the F-actin cytoskeleton, we evaluated the effects of blebbistatin, a potent myosin II inhibitor, and the corresponding agonist ionomycin, on Caco-2 monolayers. The NaF-induced reduction in TEER and increase in FD-4 penetration (Fig. 3B and Fig. 3C) were significantly reversed by the administration of blebbistatin

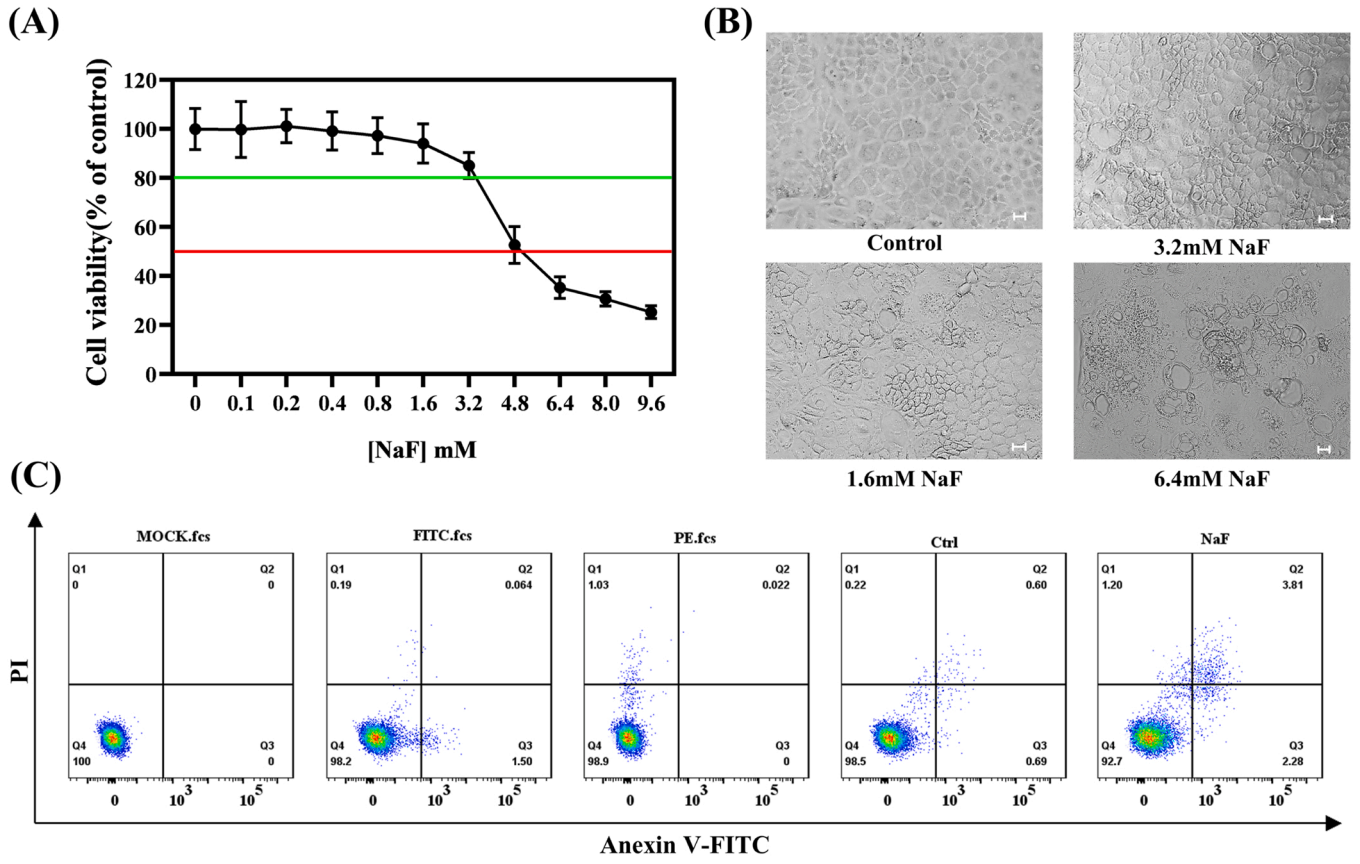

Fig. 1. NaF cytotoxicity. (A) Caco-2 viability as a function of NaF concentration. (B) Caco-2 morphology by phase-contrast microscopy. Each image is representative of three independent experiments. Scale bar = 25 μm. (C) Apoptosis measured by flow cytometry. Data are presented as means ± standard deviation (n = 3).

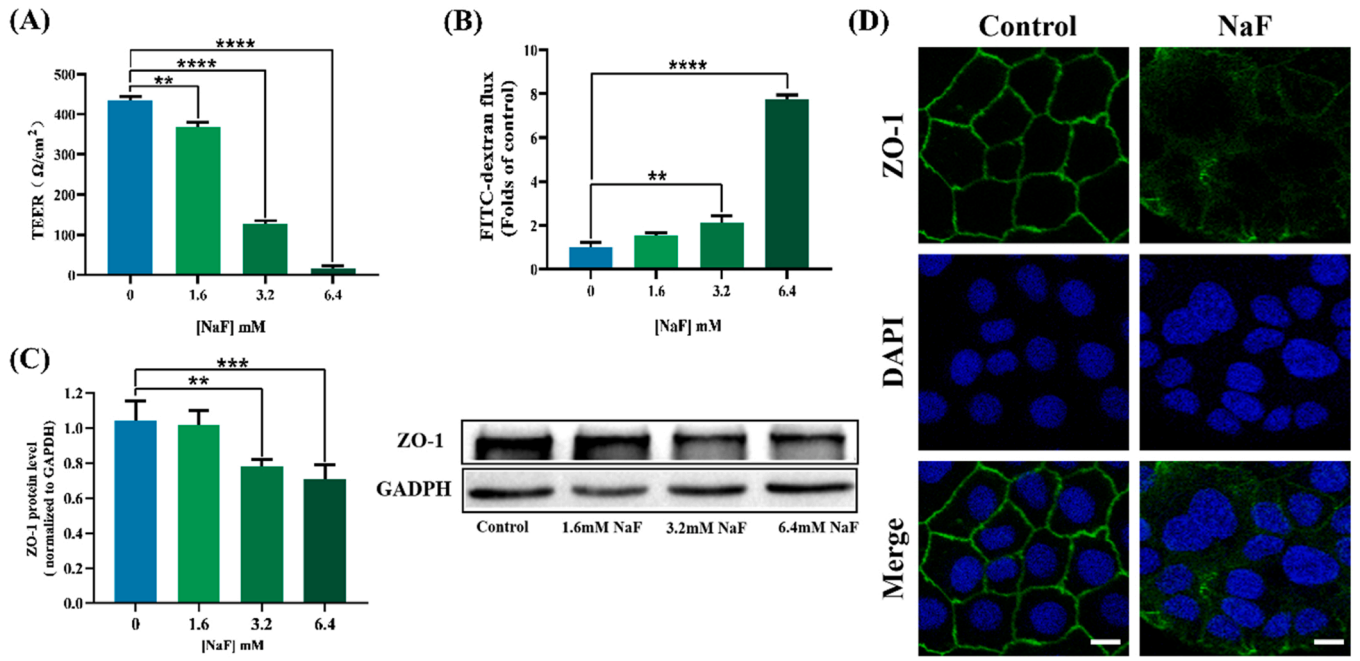

Fig. 2. NaF disruption of barriers in cultured Caco-2 intestinal cells measured by transepithelial electrical resistance (TEER) (A) and FITC-4D permeability (B). (C) Representative western blotting for TJ protein ZO-1 and quantification of integrated density normalized to GAPDH. (D) Representative immunofluorescent staining for ZO-1 (green), with nuclei co-labeled with DAPI (blue). Scale bar, 20 μm. Data are presented as means ± standard deviation (n = 3). ** $P < 0.01$, *** $P < 0.001$, and **** $P < 0.0001$ compared to control.

($P < 0.001$), almost completely restoring the barrier integrity (control vs. Bleb+NaF, $P > 0.05$). In contrast, monolayer paracellular permeability surged after treatment with ionomycin ($P < 0.0001$). In addition, studies have shown that the actin cytoskeleton of epithelial cells can adjust the stability of junctional complexes. Thus, we examined changes in F-actin (visualized with phalloidin) and the ZO-1 by immunofluorescent staining. As shown in Fig. 3D, in control cells, F-actin bundles were arranged in an orderly manner, with a small number of peripheral dense bands at the cell edge, and ZO-1 was arranged continuously around the cell membrane. And NaF or ionomycin treatments triggered inappropriate polymerization of F-actin, which in turn transformed the perijunctional actin belt into a mosaic of disorganized filaments and stress fiber-like bundles, accordingly, the fluorescence of F-actin increased by 2.37- and 1.96-fold, respectively, compared to control cells (Fig. 3E). While blebbistatin dramatically decreased intracellular F-actin content and restored ZO-1's ability to construct linear regular connections, ionomycin made an impact comparable to that of NaF. In conclusion, MLC2 phosphorylation is a crucial regulatory process in intestinal barrier breakdown mediated by NaF.

3.4. NaF activates RhoA/ROCK pathway and MLCK in Caco-2 cells

As a key governor of epithelial actin cytoskeletal dynamics, the phosphorylation of MLC-2 is predominantly mediated by Rho/ROCK pathway and MLCK (Jin and Blikslager, 2016; Zou et al., 2018). Hence, we attempt to investigate whether these pathways are involved in NaF-induced disruption of TJs and the F-actin cytoskeleton through western blotting and immunofluorescence. NaF-treated cells showed a marked increase in RhoA expression compared to controls, from (0.241 ± 0.023) to (0.950 ± 0.035) (Fig. 4A). Simultaneously, the expression of the RhoA effector kinase ROCK was elevated from (0.486 ± 0.024) to (0.854 ± 0.065), indicating a striking activation of RhoA/ROCK signaling. In addition to RhoA/ROCK, Ca^{2+}-mediated epithelial MLCK mediates MLC2 phosphorylation. Expression of the MLCK protein increased dramatically from (0.332 ± 0.131) to (1.123 ± 0.092). Similarly, immunostaining was compatible with the western blotting data. In untreated cells, both RhoA and ROCK showed diffuse irregular staining patterns without significant nuclear colocalization (Fig. 4B). In contrast, after 24 h in 3.2 mM NaF, the expression of RhoA ($P = 0.008$) and ROCK ($P < 0.0001$) increased significantly; both were enriched in the cytoplasm. The same phenomenon was observed for MLCK; an obvious increase in fluorescence intensity was observed in NaF-treated cells ($P = 0.0011$). We next tested whether inhibition of these proteins abrogates NaF-induced intestinal barrier hyperpermeability by pretreatment with the pharmacological inhibitors Rhosin, Y-27632 and ML-7 before NaF exposure. Epithelial barrier breakdown, measured by two different methods, triggered by NaF was reversed by inhibition of either RhoA/ROCK or MLCK (Fig. 5B and C). In addition, after inhibitor pretreatment ZO-1 was relocalized to cell–cell junctions, its expression was restored to normal levels, and stress fibers were dramatically decreased compared to NaF treatment alone (Fig. 5A and D). These results indicate that NaF induces barrier failure through the RhoA/ROCK pathway and MLCK.

3.5. NaF increases free intracellular Ca^{2+} in Caco-2 cells

The mechanism by which NaF activates MLCK and RhoA remains unknown. We speculate that intracellular calcium homeostasis might be involved, because increased Ca^{2+} has been shown to upregulate RhoA and MLCK (Rao et al., 2003; Shen et al., 2010). The Ca^{2+} indicator Cal 520-AM was administered to label Ca^{2+} in Caco-2 cells, and the content of $[Ca^{2+}]i$ was tested before and after 3.2 mM NaF. After 24 h of treatment, the fluorescence intensity of Ca^{2+} in the cytoplasm was enhanced obviously (Fig. 6A). To further quantify $[Ca^{2+}]i$, fluorescence intensity was measured using flow cytometry (Fig. 6B and C), showing that Cal 520-AM was (3.774 ± 0.624) times that of control cells, after treatment with 3.2 mM NaF.

3.6. Mechanism of NaF-induced increase in Ca^{2+}

Next, we investigated whether the fluoride-induced increase in $[Ca^{2+}]i$ was due to an influx from extracellular sources or a release from

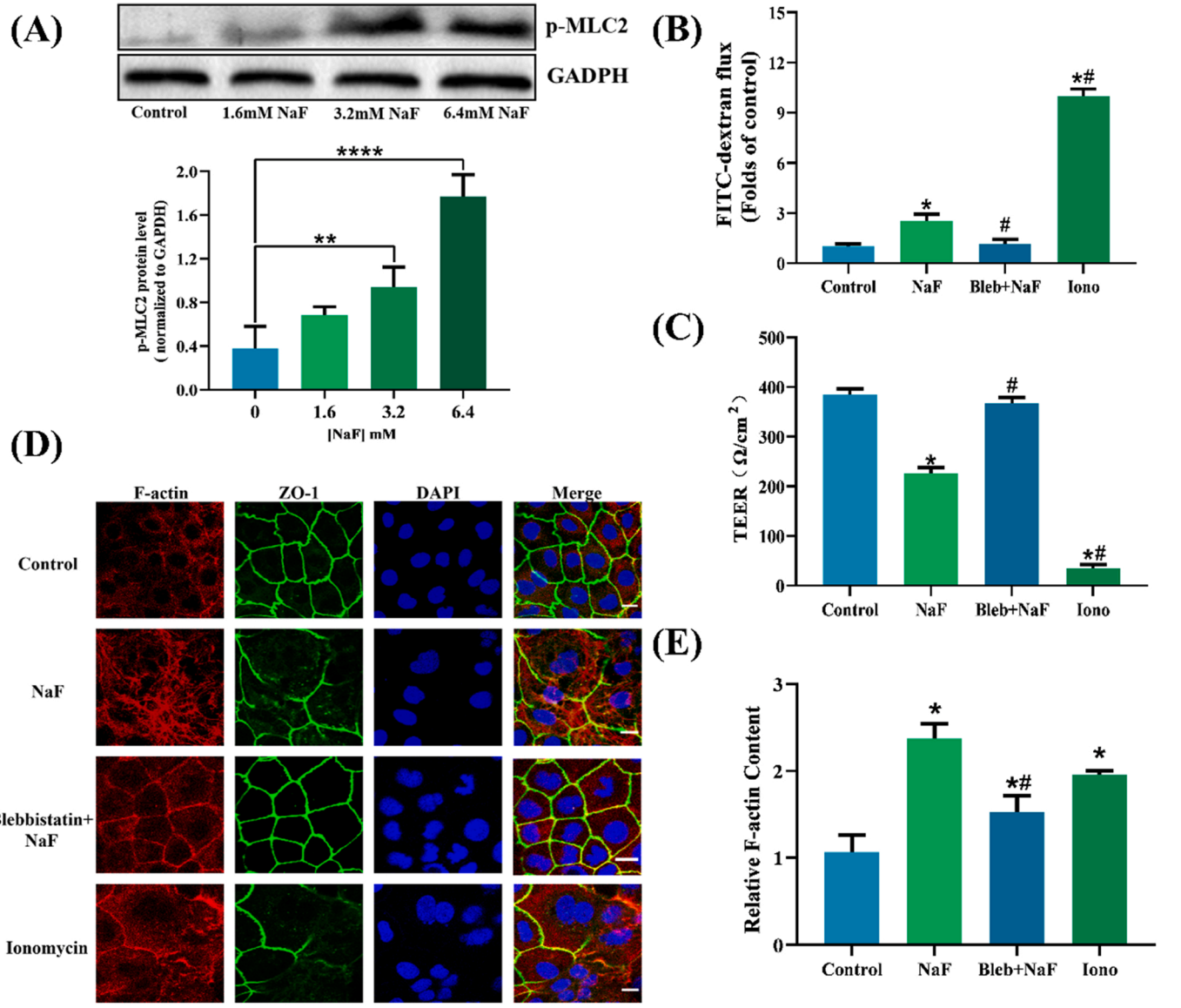

Fig. 3. NaF increases intracellular MLC phosphorylation and regulates paracellular permeability. (A) NaF alters p-MLC2 expression. Representative western blot image (top); quantification of integrated density normalized to GAPDH (bottom). Results represent means ± SD of 3 independent experiments; * $P < 0.01$, **** $P < 0.0001$ compared to control. (B and C) Measurements of barrier function using (B) TEER and (C) FITC-D4 permeability. Caco-2 monolayers were treated with 3.2 mM NaF for 24 h or ionomycin for 0.5 h, in the presence or absence of blebbistatin (50 μM) for 1 h. (D) Caco-2 stained for ZO-1 (green), F-actin (red), and nuclei (blue). Images are representative of at least 5 independent experiments. Scale bar, 20 μm. (E) Quantification of F-actin fluorescence. Results represent means ± SD of 3 independent experiments. Compared with control, * $P < 0.05$; compared with 3.2 mM NaF treatment, $^{\#}P < 0.05$.

intracellular stores. As shown in Fig. 7A, compared with NaF-treated control cells, pretreatment with the nonspecific intracellular calcium chelator BAPTA-AM significantly blocked the increase of $[Ca^{2+}]i$ caused by NaF ($P = 0.0115$), while extracellular calcium chelator EGTA ($P = 0.4132$) did not attenuate it. Meanwhile, NaF noticeably diminished TEER and increased FD-4 permeability (Fig. 7B; both $P < 0.0001$ vs. control), which was ameliorated after chelation by BAPTA-AM (Fig. 7B; both $P < 0.0001$ vs. NaF) and almost the same as the level in untreated cells (both $P > 0.1$ vs. control). Additionally, immunofluorescence staining showed that BAPTA-AM pretreatment abrogated the NaF-induced redistribution of ZO-1 and the assembly of stress fibers (Fig. 7 C). To further verify the impact of chelating intracellular calcium ions on the RhoA/ROCK signaling pathway and MLCK, upstream proteins were labeled with green fluorescence. Our results showed that the overexpression of RhoA and MLCK, initially triggered by NaF, decreased to that of the control state (Fig. 7D). However, these improvements were not observed after EGTA pretreatment. Finally, western blotting showed that NaF-induced ZO-1 downregulation was reversed in cells pretreated with BAPTA-AM, Rhosin, or ML-7 (Fig. 7E) (both $P < 0.001$ vs. NaF, $P > 0.05$ vs. control), providing a molecular mechanism for the restoration of barrier integrity.(Fig. 8).

4. Discussion

As a ubiquitous halogen, fluoride contaminates groundwater and food to threaten human health worldwide (Rafique et al., 2015). As over 60% of fluoride is absorbed by the digestive tract (Dec et al., 2017), gastrointestinal disorders caused by fluoride have been widely confirmed. Our previous study showed that high fluoride exposure enhanced gut permeability, with TJ downregulation in mice (Xin et al., 2021b), which consistent with another study (Li et al., 2020). However, the exact mechanism by which fluoride causes intestinal barrier impairment remains to be elucidated. This study aims to investigate the adverse effects of fluoride on the tight junction protein and actin

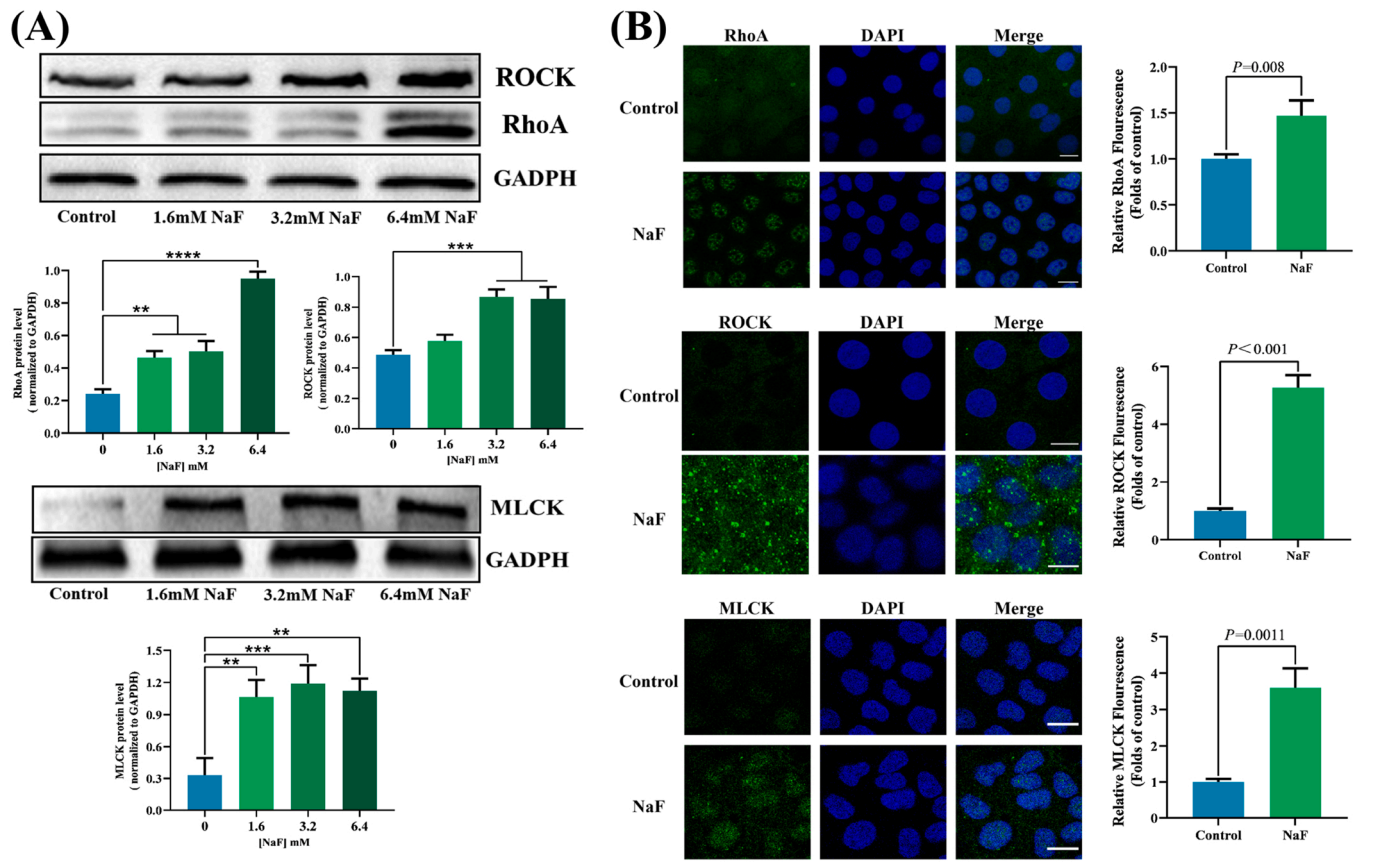

Fig. 4. Rho/ROCK and MLCK activation mediates NaF-induced disruption of Caco-2 TJs. (A) Effect of NaF on the expression of Rho, ROCK, and MLCK. Representative western blot images (top); quantification of integrated density normalized to GAPDH (bottom). Results represent means ± SD of 3 independent experiments. ** $P < 0.01$, *** $P < 0.001$, **** $P < 0.0001$ compared to control. (B) Left, representative immunofluorescence staining for RhoA, ROCK, and MLCK, with nuclei counterstained with DAPI. Scale bar, 20 μm. Right, quantification of fluorescence intensities. Data are presented as means ± standard deviation (n = 5). ** $P < 0.01$, *** $P < 0.001$, **** $P < 0.0001$ as compared to control.

cytoskeleton using cultured cell.

As a useful model for appraising intestinal function, Caco-2 cells show differentiation and polarity similar to those of human intestinal epithelioid cells (Sun et al., 2008). After culturing on a permeable polycarbonate membrane, cells contact each other and polarize as a confluent monolayer. Caco-2 monolayers have the same TJs as small intestinal epithelial cells, and are similar to human small intestinal epithelial cells in morphology, ion transport, and marker gene expression (Lea, 2015). Although Caco-2 cells cannot directly simulate in vivo conditions, they have many advantages that make them widely used in studies of intestinal epithelial barriers (Liu et al., 2021; Zhao et al., 2021). Polarized epithelial cells formed mucosal surfaces that protect mammalian hosts from the external environment, however, if the homeostasis is disrupted, intestinal microbes or their metabolites pose risks of infection and inflammation (Peterson and Artis, 2014). Animal experiments have shown that fluoride overexposure damages intestinal tissue structure and inhibits the proliferation of epithelial cells (Wang et al., 2020). In the present study, CCK-8 assay and flow cytometry analysis confirmed the cytotoxic effects of NaF on Caco-2 cells. We also documented alterations in morphology; high fluoride exposure induced irregular expansion of cells, appearance of internal vacuoles, and even ablation.

As an important line of defense for the organism, the intestinal barrier mitigates some naturally occurring toxins and food contaminants, as well as ingested bacterial and viral pathogens (Camilleri et al., 2012). “Intestinal leakage” refers to the compromised integrity of the intestinal barrier, characterized by an increase in the permeability, which allows the entry of toxic substances from the enteric cavity into the bloodstream. In the present study, fluoride treatment significantly reduced barrier function by two different assays, TEER and the paracellular passage of FD-4, standard parameters for measuring the integrity of epithelial barriers (Pinton et al., 2009). Consistent with our observation, Amadeu de Oliveira et al. (Amadeu de Oliveira et al., 2018) showed that fluoride disrupts rat colonic epithelial barrier and alters transepithelial ion transport. Similarly, NaF enhances gut penetrability in mice, manifested by elevated serum DAO activity and (D-LA) content, indicators of mucosal integrity (Li et al., 2020). Given that the intimate relevance between cell death and barrier collapse (Flynn and Buret, 2008), the experimental NaF dose should exclude Caco-2 monolayer hyperpermeability resulting from the cell death pathway as much as possible. Although 3.2 mM NaF did not significantly reduce Caco-2 cell viability, TEER decreased and FD-4 infiltration increased under this condition.

The permeability of the intestinal barrier primarily depends on the integrity of TJs between adjacent cells. In contrast to adherens junctions, which initiate cell–cell contacts and control tensile force, TJs act as paracellular gates to confine the trafficking of molecules based on their sizes and charges (Bhat et al., 2018). TJ disruption mirrored epithelial integrity loss, which triggers multiple diseases that endanger health (Wu et al., 2016; Xin et al., 2021a). We found that NaF administration significantly decreased expression of the scaffolding protein ZO-1. Consistently, NaF, administered at 100 ppm in drinking water, remarkably reduced the mRNA and/or protein levels of ZO-1 in the ileum of mice (Xin et al., 2021b). Additionally, 1 mM fluoride impeded TJ formation in rat ameloblast HAT-7 cells (Rácz et al., 2017). TJ function is also critically governed by subcellular localization. The

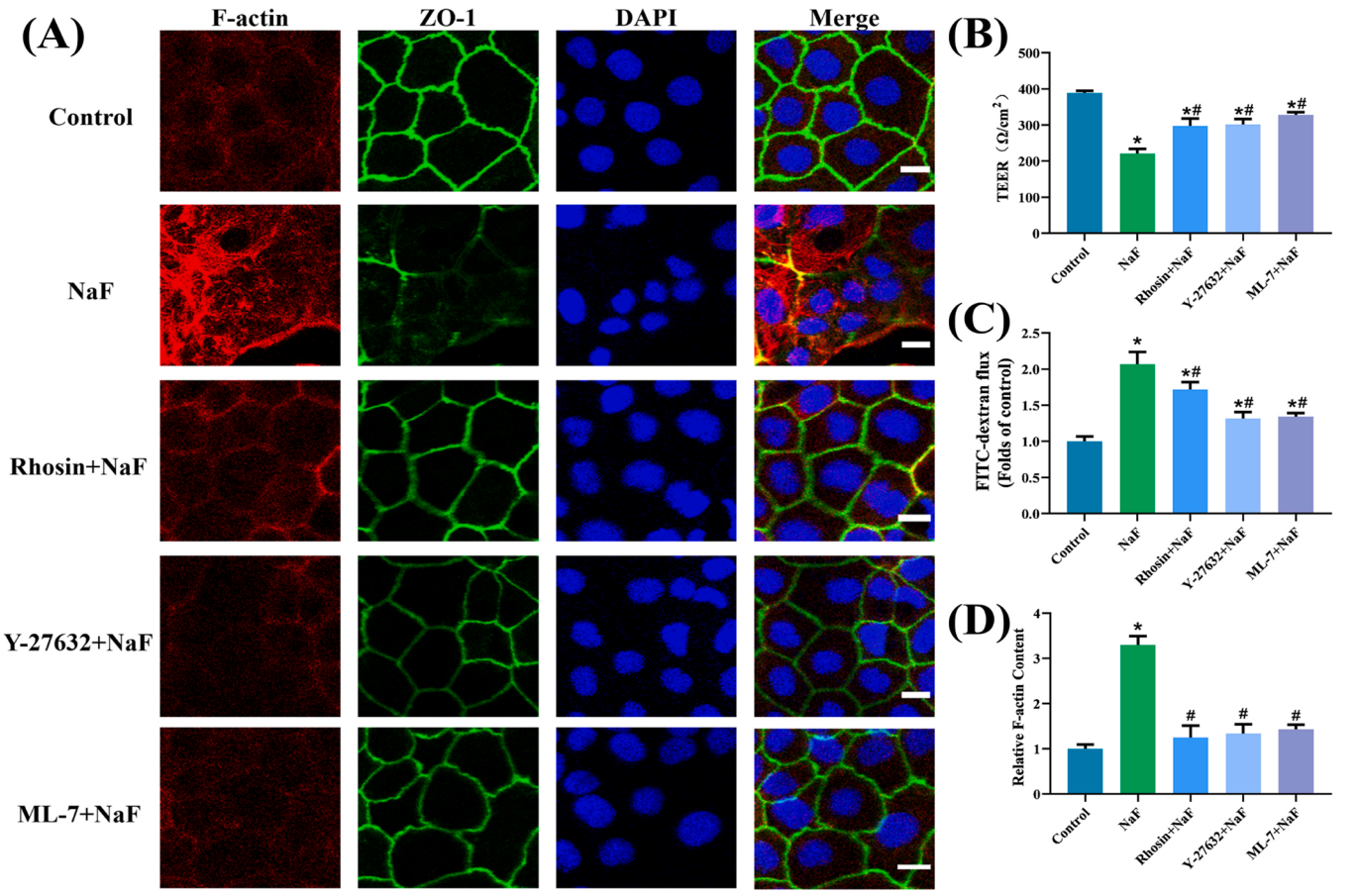

Fig. 5. Inhibition of Rho/ROCK and MLCK ameliorates NaF-induced stress fiber formation and intestinal barrier hyperpermeability in Caco-2 cell monolayers. Cells were pretreated with 40 μM Rhosin, 40 μM Y27632, or 10 μM ML-7 for 1 h, followed by treatment with 3.2 mM NaF for 24 h. (A) Representative images of F-actin (red), and immunofluorescence staining for ZO-1 (green), with nuclei counterstained with DAPI (blue). Scale bar = 20 μm. Effects of inhibition on TEER (B), FITC-4D permeability (C), and F-actin (D). Data are presented as means ± standard deviation (n = 3). Compared with control, * $P < 0.05$; compared with 3.2 mM NaF treatment, $^{\#}P < 0.05$.

rearrangement of TJs has been reported to favor barrier hyperpermeability (Rahner et al., 2001). However, most studies on the correlation between fluoride and TJs have been limited to protein quantification. As confocal microscopy can capture subtle changes in target proteins, we observed that NaF noticeably interfered with the continuity of ZO-1 distribution. In agreement with these data, Wang (Wang et al., 2018) found that Ochratoxin A-treated IPEC-J2 monolayers exhibited irregular ZO-1 staining patterns and barrier dysfunction. Another study showed that bradykinin-mediated blood-tumor barrier (BTB) resulted from the redistribution of ZO-1 (Liu et al., 2008).

Although we demonstrated NaF-induced barrier failure, the exact mechanism remains unclear. TJs are linked to the cytoskeleton; tightly regulated actomyosin dynamics play a vital role in TJ-depended epithelial barrier integrity (Takeichi, 2014). ZO-1 is coupled to actin via its C-terminus (Schneeberger and Lynch, 2004), and that ZO-1 remodeling is closely connected to contraction of the perijunctional actomyosin ring, which is largely driven by the phosphorylation of MLC2 (Jin and Blikslager, 2020). Multiple digestive diseases characterized by "Intestinal leakage" are associated with this mechanism (Buckley and Turner, 2018). Hence, we speculated that MLC2 is involved in NaF-induced barrier impairment and TJ disruption. Our data showed that NaF markedly upregulated p-MLC2. This observation is in line with another study demonstrating that treatment with 20 mM NaF for 60 min induced a seven-fold increase in p-MLC in endothelial cells, which precedes EC barrier dysfunction (Wang et al., 2001). Meanwhile, we found that blebbistatin attenuated the redistribution of ZO-1 and stress fiber assembly, while restoring the cellular barrier. In contrast, ionomycin exhibits a destructive effect comparable to that of NaF, indicating that p-MLC2 severs as an effector. Zhao (Zhao et al., 2021) also reported that imidacloprid increases paracellular permeability by upregulating p-MLC in mice. However, further experiments should be conducted to determine whether other cell adhesion proteins, such as E-cadherin or β-catenin, are subject to NaF-induced cytoskeleton rearrangement and contribute to the barrier damage.

The phosphorylation of MLC2 is dominantly mediated by Rho/ROCK pathway and MLCK (Jin and Blikslager, 2016; Zou et al., 2018). As classical members of the Rho family, RhoA and its downstream effector ROCK have been shown to influence F-actin polymerization and depolymerization (Aslam et al., 2013), participating in multiple cytoskeleton-driven cellular events (Li et al., 2018). A growing amount of research has shed light on the regulation of barrier function by Rho GTPases (Nusrat et al., 1995). Indeed, an elegant balance in Rho activity is required to guarantee optimal TJ function (Bruewer et al., 2006). ROCK can directly phosphorylate MLC2, while inhibiting p-MLC2 dephosphorylation by inactivating MCL phosphatase (MLCP) (Jin and Blikslager, 2020). Conversely, ROCK inhibition downregulates p-MLC2 and attenuates actin filament reconfiguration. Overexpression of RhoA and ROCK indicated that NaF activated the RhoA/ROCK signaling in Caco-2 cells. Meanwhile, inhibitor experiments further confirmed that NaF triggered barrier dysfunction through the RhoA/ROCK pathway. Consistent with our results, NaF co-exposure enhanced RhoK and p-MLC levels in endothelial cells (Wang et al., 2001). In addition, Yang and colleagues reported that fluoride induces contraction of isolated rat aortas by activating RhoA/Rho kinase signaling (Yang et al., 2010).

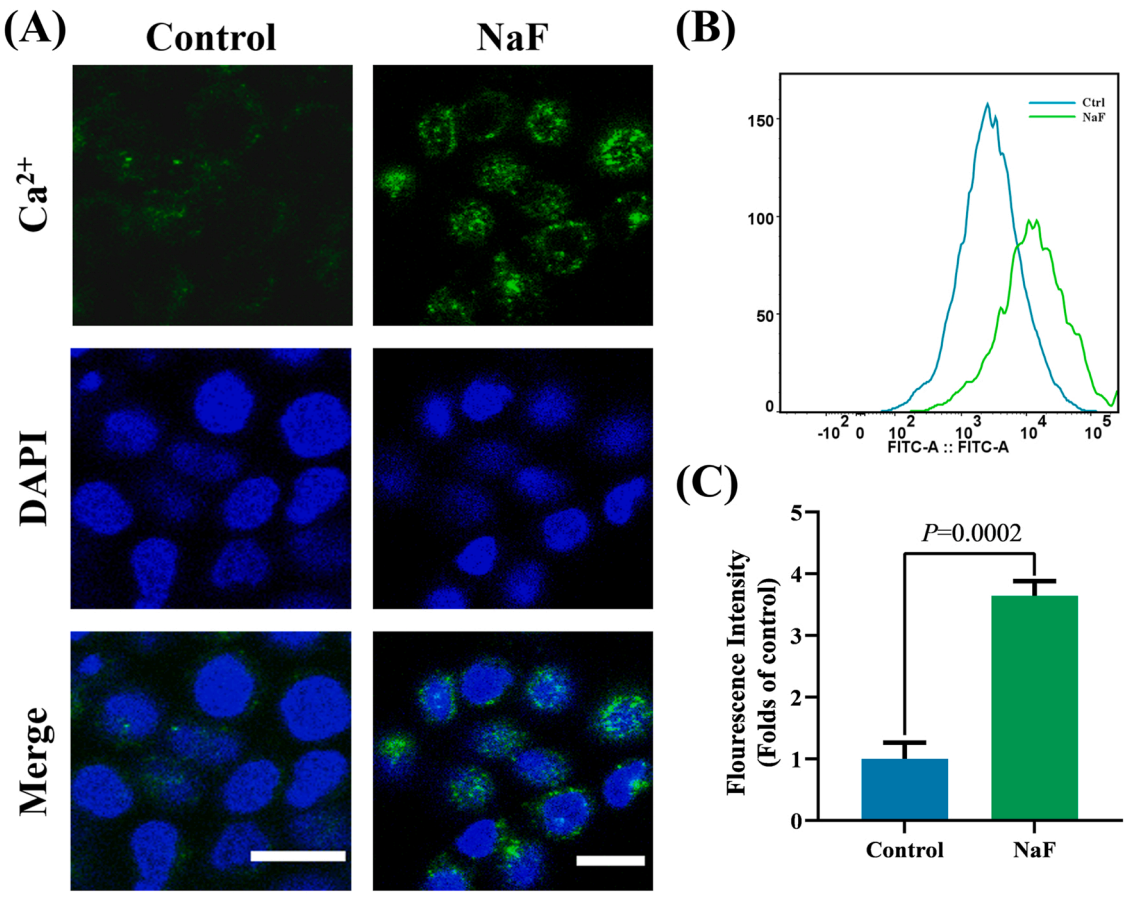

Fig. 6. NaF increases free intracellular Ca^{2+} in Caco-2 cell monolayers. (A) Ca^{2+} staining 60 min following Cal 520-AM loading, with and without 3.2 mM NaF. Scale bar, 20 μm. (B) Quantification of free intracellular Ca^{2+} by flow cytometry. (C) Quantification of Cal 520-AM fluorescence; arbitrary scale with control set to 1. Results represent means ± SD of 3 independent experiments.

Blocking RhoA/ROCK pathway protected the integrity of the intestinal barrier and hindered stress-fiber assembly in rats with chronic colitis (Zhang et al., 2021). Moreover, Zhang et al. (Zhang et al., 2013) reported that transforming growth factor (TGF) reduced both the transcription and translation level of ZO-1 via Rho/ROCK pathway, so we speculated that NaF-induced ZO-1 downregulation might relate to this.

MLC is phosphorylated by MLCK at threonine-18 and/or serine-19 (Zahs et al., 2012). Mice with MLCK deficiency, as well as those administrated with enzymatic inhibitors, exhibited attenuated barrier breakdown and fluid secretion, suggesting that MLCK is a pivotal component in pathological barrier dysfunction (Clayburgh et al., 2004). Moreover, it has been shown that the potential mechanism underlying ethanol-induced blood-brain barrier damage is oxidative stress-dependent MLCK activation (Haorah et al., 2007). In the present study, NaF treatment markedly increased MLCK expression. The inhibitor ML-7 abrogated NaF-induced TJs disruption and barrier hyperpermeability. However, this result differs from those of earlier reports. Wang and colleagues found that ML-7 failed to impede NaF-induced MLC phosphorylation, F-actin remodeling, and TEER reduction in endothelial cells (Wang et al., 2001). In addition to using different cell lines, we hypothesized that this discrepancy could be primarily attributed to the selected NaF dosage; Wang et al. used acute high-concentration fluoride exposure, whereas we adopted a relatively safe dose for longer-term treatment. Moreover, recent studies suggest that a crosslink between the MLCK and Rho/ROCK pathways cannot be excluded, because the Rho/ROCK pathway may also regulate MLCK activity through other signaling pathways, such as protein kinase C or MAPK (Anjum, 2018). Furthermore, Kazakova and colleagues verified that MLCK-mediated MLC phosphorylation requires ROCK assistance, which weakens MLCP activity (Kazakova et al., 2020).

So far, the mechanism underlying the activation of the RhoA/ROCK and MLCK pathways by NaF remains uncertain. Calcium ions are known to be upstream regulators of RhoA and MLCK (Rao et al., 2003; Shen et al., 2010). Mitochondrial dysfunction resulting in oxidative stress is a common feature of fluorosis, which in turn destroys the membrane of endoplasmic reticulum (ER) to release intracellular calcium ions (Aulestia et al., 2020). We found that NaF significantly elevated $[Ca^{2+}]_i$ levels in Caco-2 cells. Our findings are consistent with prior research showing that NaF increases calcium accumulation in renal epithelial cells (Murao et al., 2000). Indeed, $[Ca^{2+}]_i$ overload may result from the opening of plasma-membrane calcium channels and/or discharge from the ER, which serves as a cellular calcium pool (Xu et al., 2007). To our observation, BAPTA-AM, not EGTA, significantly abrogated the $[Ca^{2+}]_i$ enhancement, indicating that the increased $[Ca^{2+}]_i$ originated from the release of intracellular calcium stores. Similar to our results, BAPTA-AM pretreatment rescued fluorine-induced elevations in $[Ca^{2+}]_i$, ROS, and LDH in human neuroblastoma cells (Xu et al., 2013). In addition, $[Ca^{2+}]_i$ overload compromises TJ integrity and decreases TEER in Caco-2 monolayers (Martinez-Palomo et al., 1980). In this study, BAPTA-AM corrected the epithelial integrity loss and stress-fiber formation; it also inhibited the activation of RhoA and MLCK. Our results suggest that $[Ca^{2+}]_i$ acts upstream of RhoA and MLCK, which in turn mediates actomyosin contraction. Consistent with these data, Elamin (Elamin et al., 2014) found that ethanol-driven $[Ca^{2+}]_i$ discharge upregulated Rho/ROCK signaling in Caco-2 cells, impairing epithelial barrier function. Another study showed that $[Ca^{2+}]_i$ and ROS play essential roles in MLCK-mediated MLC phosphorylation (Wu et al., 2020). Nevertheless, our data indicate that $[Ca^{2+}]_i$-dependent signaling has not been fully

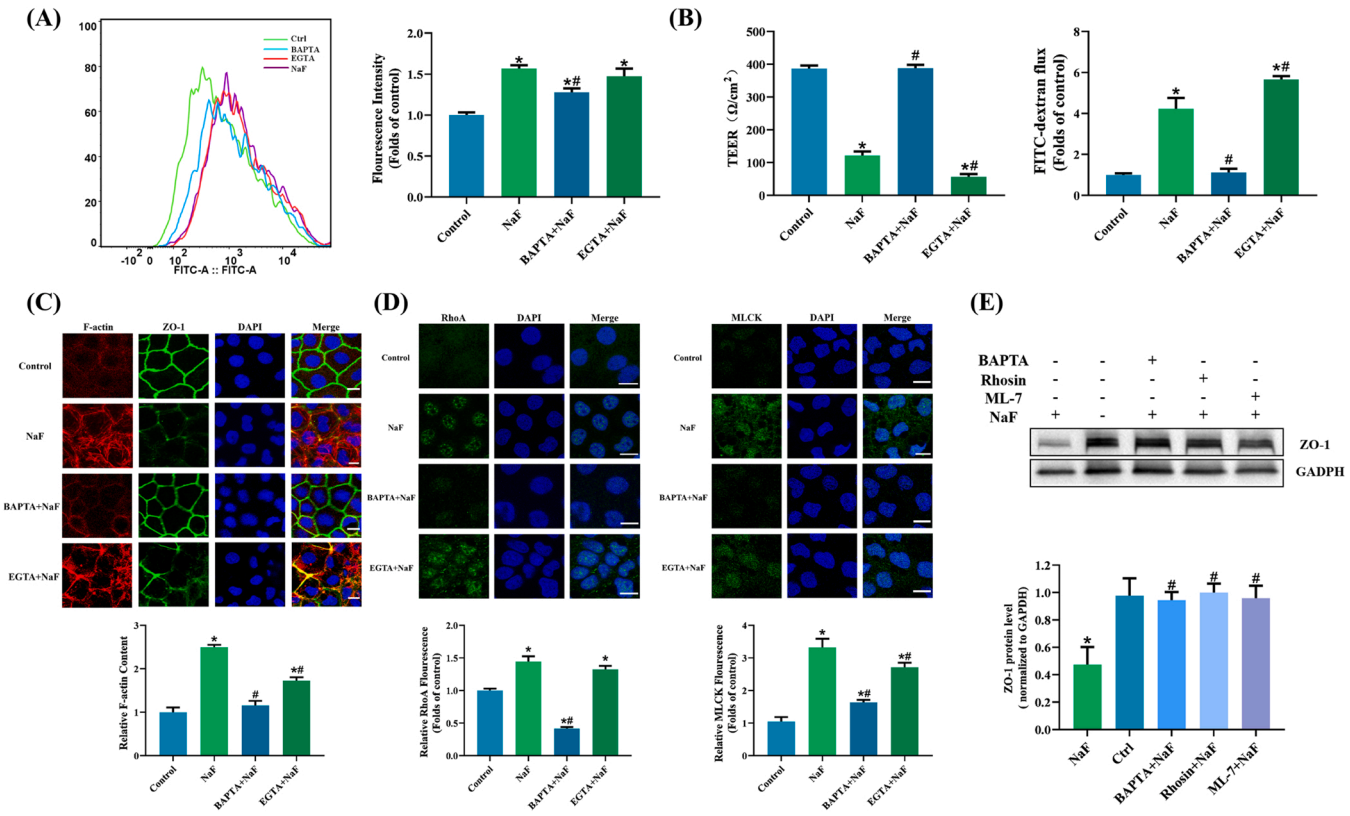

Fig. 7. Mechanism of NaF-induced increase in Ca^{2+} in Caco-2 cells pretreated with the intracellular calcium chelator BAPTA-AM (15 μM) or extracellular calcium chelator EGTA (4 mM) for 1 h, followed by treatment with NaF (3.2 mM) for 24 h. (A) Intracellular calcium levels in Caco-2 cells detected using fluorescence intensity of Cal 520-AM measured by flow cytometry (left); quantification of fluorescence intensities (right). (B) Effects of chelation on TEER (left) and FITC-4D permeability (right). (C) Effects of chelation on F-actin (red) and immunofluorescent staining for ZO-1 (green), with nuclei counterstained with DAPI (blue). Scale bar, 20 mm. Quantification of F-actin is shown below. (D) Effect of chelation on expression of RhoA and MLCK. Representative micrographs of RhoA (green, left) or MLCK (green, right), and nuclei stained with DAPI. Images are representative of at least 5 independent experiments. Scale bar, 20 μm. Quantifications are shown below. (E) Representative western blot and integrated density quantification of ZO-1 GAPDH as an internal reference. Data are presented as means ± standard deviation (n = 3). Compared with control, * $P < 0.05$; compared with the 3.2 mM NaF treatment, $^{\#}P < 0.05$.

elucidated, because BAPTA-AM chelation produced disparate down-regulation of RhoA and MLCK; therefore, we hypothesize that alternative pathways may be involved in their adjustments. Interestingly, we discovered that $[Ca^{2+}]_i$ and p-MLC2 play predominant roles in NaF-induced barrier hyperpermeability, as blebbistatin and BAPTA-AM treatment almost completely restored the integrity of Caco-2 monolayers, which is better than both the RhoA/ROCK and MLCK inhibitors.

Collectively, the enhancement of $[Ca^{2+}]i$ resulted from the intracellular compartment release, and $[Ca^{2+}]_i$ plays an important role in NaF-mediated RhoA and MLCK activation. Suppression of RhoA with Rhosin, or MLCK with ML-7, and chelation of overloaded $[Ca^{2+}]_i$ with BAPTA-AM, rescued NaF-induced cytoskeleton/TJ alterations and subsequent epithelial barrier breakdown.

5. Conclusion

Collectively, our results highlight the important role of NaF in promoting Caco-2 monolayers hyperpermeability via the activation of RhoA/ROCK signaling and MLCK by releasing intracellular calcium ion. Moreover, this study sheds light on the role of MLC2 phosphorylation in NaF-induced TJ disruption and actin filament remodeling, which may provide a potential therapeutic targets for high-fluoride exposure-related intestinal injury. However, other relationships between the RhoA/ROCK pathway and MLCK may remain to be identified. It is necessary to extend our current knowledge to animal models or intestinal specimens from patients with fluorosis by detecting alterations in signaling proteins and calcium.

Funding

This work is supported by National Natural Science Foundation of China (Grant No: 82204045), Guangdong Basic and Applied Basic Research Foundation (Grant No: 2020A1515110693) and Scientific Development funds for Natural Science Foundation of Guangdong Province, China (Grant No: 2022A1515011625, 2022A1515011230).

CRediT authorship contribution statement

Lianxin Li: Project administration, Formal analysis, Writing - original draft, Writing - review & editing. **Jinge Xin:** Project administration, Software. **Hesong Wang:** Investigation, Writing - original draft. **Weiqi Peng:** Writing – review & editing. **Yanxi Zhou:** Project administration, Writing - original draft. **Xingmei Liu:** Formal analysis. **Yu Lin:** Methodology. **Jing Fang:** Methodology. **Bo Jing:** Software. **Kangcheng Pan:** Conceptualization, Methodology. **Yan Zeng:** Conceptualization, Methodology. **Dong Zeng:** Conceptualization, Methodology. **Xiang Qin:** Methodology, Writing - review & editing. **Yang Bai:** Writing – review & editing. **Xueqin Ni:** Writing – review & editing.

Declaration of Competing Interest

The authors declare that they have no known competing financial interests or personal relationships that could have appeared to influence the work reported in this paper.

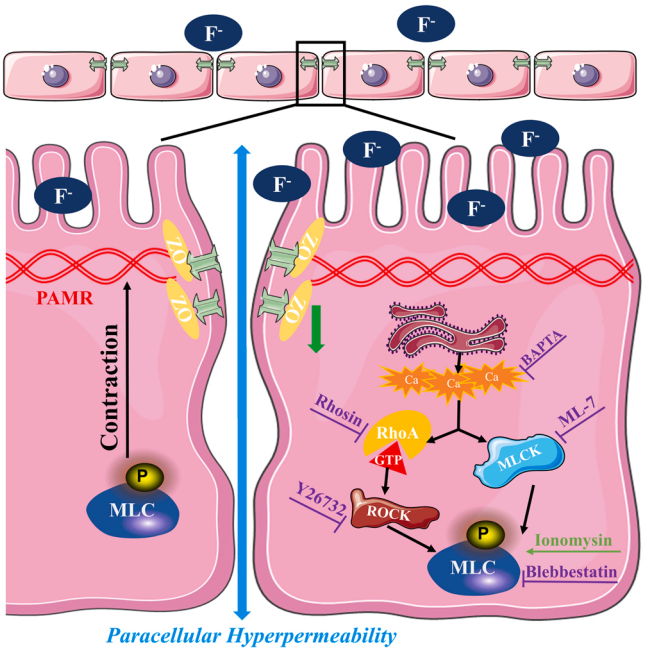

Fig. 8. Model of NaF-induced intestinal barrier disruption. Overloaded intracellular Ca^{2+} in epithelial cells activates RhoA/ROCK pathway and MLCK, increasing phosphorylation of MLC2, stimulating F-actin aggregation, stress-fiber formation, cell contraction, and TJ disruption. GTP, Guanosine triphosphate; MLC, myosin light chain; MLCK, myosin light chain kinase; PAMR, Perijunctional F-actin ring; RhoA, Ras homologue gene family member A; ROCK, Rho-associated protein kinase; TJ, tight junction; ZO, Zonula occludens.

Data Availability

Data will be made available on request. Supplementary data to this article can be found at Supplementary file 1.

Appendix A. Supporting information

Supplementary data associated with this article can be found in the online version at doi:10.1016/j.ecoenv.2023.114940.

References

Al Nabhani, Z., et al., 2017. Complementary roles of Nod2 in hematopoietic and nonhematopoietic cells in preventing gut barrier dysfunction dependent on MLCK activity. Inflamm. Bowel Dis. 23, 1109–1119.

Amadeu de Oliveira, F., et al., 2018. The effect of fluoride on the structure, function, and proteome of intestinal epithelia. Environ. Toxicol. 33, 63–71.

Anjum, I., 2018. Calcium sensitization mechanisms in detrusor smooth muscles. J. Basic Clin. Physiol. Pharm. 29, 227–235.

Arnold, T.R., et al., 2017. Rho GTPases and actomyosin: partners in regulating epithelial cell-cell junction structure and function. Exp. Cell Res 358, 20–30.

Aslam, M., et al., 2013. Hypoxia-reoxygenation-induced endothelial barrier failure: role of RhoA, Rac1 and myosin light chain kinase. J. Physiol. 591, 461–473.

Aulestia, F.J., et al., 2020. Fluoride exposure alters Ca(2+) signaling and mitochondrial function in enamel cells. Sci. Signal 13.

Balda, M.S., et al., 1991. Assembly and sealing of tight junctions: possible participation of G-proteins, phospholipase C, protein kinase C and calmodulin. J. Membr. Biol. 122, 193–202.

Bhat, A.A., et al., 2018. Tight junction proteins and signaling pathways in cancer and inflammation: a functional crosstalk. Front Physiol. 9, 1942.

Bruewer, M., et al., 2006. Inflammatory bowel disease and the apical junctional complex. Ann. N. Y Acad. Sci. 1072, 242–252.

Buckley, A., Turner, J.R., 2018. Cell biology of tight junction barrier regulation and mucosal disease. Cold Spring Harb. Perspect. Biol. 10.

Cáceres, M., et al., 2005. Overexpression of RhoA-GTP induces activation of the epidermal growth factor receptor, dephosphorylation of focal adhesion kinase and increased motility in breast cancer cells. Exp. Cell Res. 309, 229–238.

Camilleri, M., et al., 2012. Intestinal barrier function in health and gastrointestinal disease. Neurogastroenterol. Motil. 24, 503–512.

Campos, S.B., et al., 2009. Cytokine-induced F-actin reorganization in endothelial cells involves RhoA activation. Am. J. Physiol. Ren. Physiol. 296, F487–F495.

Capaldo, C.T., Nusrat, A., 2009. Cytokine regulation of tight junctions. Biochim. Biophys. Acta 1788, 864–871.

Chen, J., et al., 2021. Hydrogeochemical evidence for fluoride behavior in groundwater and the associated risk to human health for a large irrigation plain in the Yellow River Basin. Sci. Total Environ. 800, 149428.

Choubisa, S.L., Choubisa, D., 2016. Status of industrial fluoride pollution and its diverse adverse health effects in man and domestic animals in India. Environ. Sci. Pollut. Res. Int 23, 7244–7254.

Clayburgh, D.R., et al., 2004. A differentiation-dependent splice variant of myosin light chain kinase, MLCK1, regulates epithelial tight junction permeability. J. Biol. Chem. 279, 55506–55513.

Cunningham, K.E., Turner, J.R., 2012. Myosin light chain kinase: pulling the strings of epithelial tight junction function. Ann. N. Y Acad. Sci. 1258, 34–42.

Dec, K., et al., 2017. The influence of fluorine on the disturbances of homeostasis in the central nervous system. Biol. Trace Elem. Res 177, 224–234.

Dionizio, A., et al., 2020. Effects of acute fluoride exposure on the jejunum and ileum of rats: Insights from proteomic and enteric innervation analysis. Sci. Total Environ. 741, 140419.

Ducibella, T., Fissore, R., 2008. The roles of Ca2+, downstream protein kinases, and oscillatory signaling in regulating fertilization and the activation of development. Dev. Biol. 315, 257–279.

Ebert, B., et al., 2005. Identification of BCRP as transporter of benzo[a]pyrene conjugates metabolically formed in Caco-2 cells and its induction by Ah-receptor agonists. Carcinogenesis 26, 1754–1763.

Elamin, E., et al., 2014. Ethanol disrupts intestinal epithelial tight junction integrity through intracellular calcium-mediated Rho/ROCK activation. Am. J. Physiol. Gastrointest. Liver Physiol. 306, G677–G685.

Fein, N.J., Cerklewski, F.L., 2001. Fluoride content of foods made with mechanically separated chicken. J. Agric. Food Chem. 49, 4284–4286.

Flynn, A.N., Buret, A.G., 2008. Caspases-3, -8, and -9 are required for induction of epithelial cell apoptosis by enteropathogenic E. coli but are dispensable for increased paracellular permeability. Micro Pathog. 44, 311–319.

Fung, K.F., et al., 1999. Fluoride contents in tea and soil from tea plantations and the release of fluoride into tea liquor during infusion. Environ. Pollut. 104, 197–205.

Haorah, J., et al., 2007. Oxidative stress activates protein tyrosine kinase and matrix metalloproteinases leading to blood-brain barrier dysfunction. J. Neurochem 101, 566–576.

Jaffe, A.B., Hall, A., 2005. Rho GTPases: biochemistry and biology. Annu. Rev. Cell Dev. Biol. 21, 247–269.

Jha, P.K., Tripathi, P., 2021. Arsenic and fluoride contamination in groundwater: A review of global scenarios with special reference to India. Groundw. Sustain. Dev. 13.

Jiang, Y., et al., 2021. bFGF ameliorates intestinal mucosal permeability and barrier function through tight junction proteins in burn injury rats. Burns 47, 1129–1136.

Jin, Y., Blikslager, A.T., 2016. Myosin light chain kinase mediates intestinal barrier dysfunction via occludin endocytosis during anoxia/reoxygenation injury. Am. J. Physiol. Cell Physiol. 311, C996–c1004.

Jin, Y., Blikslager, A.T., 2020. The regulation of intestinal mucosal barrier by myosin light Chain Kinase/Rho Kinases. Int. J. Mol. Sci. 21.

Job, J.T., et al., 2021. Toxic effects of fluoride in intestinal epithelial cells and the mitigating effect of methanol extract of coconut haustorium by enhancing de novo glutathione biosynthesis. Environ. Res 200, 111717.

Kazakova, O.A., et al., 2020. MLCK and ROCK mutualism in endothelial barrier dysfunction. Biochimie 168, 83–91.

Lea, T., 2015. Caco-2 Cell Line. In: Verhoeckx, K., et al. (Eds.), The Impact of Food Bioactives on Health: in vitro and ex vivo models. Springer, pp. 103–111. Copyright 2015, The Author(s). Cham (CH).

Li, M., et al., 2020. Self-recovery study of the adverse effects of fluoride on small intestine: Involvement of pyroptosis induced inflammation. Sci. Total Environ. 742, 140533.

Li, Z., et al., 2018. Naringin attenuates MLC phosphorylation and NF-κB activation to protect sepsis-induced intestinal injury via RhoA/ROCK pathway. Biomed. Pharm. 103, 50–58.

Liu, G., et al., 2021. Tryptophan ameliorates barrier integrity and alleviates the inflammatory response to enterotoxigenic Escherichia coli K88 through the CaSR/Rac1/PLC-γ1 signaling pathway in porcine intestinal epithelial cells. Front. Immunol. 12, 748497.

Liu, L.B., et al., 2008. Bradykinin increases blood-tumor barrier permeability by down-regulating the expression levels of ZO-1, occludin, and claudin-5 and rearranging actin cytoskeleton. J. Neurosci. Res 86, 1153–1168.

Mahdavi, K., et al., 2022. Enhanced photocatalytic degradation of toxic contaminants using Dy(2)O(3)-SiO(2) ceramic nanostructured materials fabricated by a new, simple and rapid sonochemical approach. Ultrason Sonochem. 82, 105892.

Martinez-Palomo, A., et al., 1980. Experimental modulation of occluding junctions in a cultured transporting epithelium. J. Cell Biol. 87, 736–745.

Matsuo, S., et al., 2000. Fluoride-induced ultrastructural changes in exocrine pancreas cells of rats: fluoride disrupts the export of zymogens from the rough endoplasmic reticulum (rER). Arch. Toxicol. 73, 611–617.

Miranda, G.H.N., et al., 2018. Chronic exposure to sodium fluoride triggers oxidative biochemistry misbalance in mice: effects on peripheral blood circulation. Oxid. Med. Cell Longev. 2018, 8379123.

Mirza, H., et al., 2012. Statin pleiotropy prevents rho kinase-mediated intestinal epithelial barrier compromise induced by Blastocystis cysteine proteases. Cell Microbiol 14, 1474–1484.

Murao, H., et al., 2000. Sodium fluoride increases intracellular calcium in rat renal epithelial cell line NRK-52E. Biol. Pharm. Bull. 23, 581–584.

Nigam, S.K., et al., 1992. Changes in intracellular calcium during the development of epithelial polarity and junctions. Proc. Natl. Acad. Sci. USA 89, 6162–6166.
Nusrat, A., et al., 1995. Rho protein regulates tight junctions and perijunctional actin organization in polarized epithelia. Proc. Natl. Acad. Sci. USA 92, 10629–10633.
Peterson, L.W., Artis, D., 2014. Intestinal epithelial cells: regulators of barrier function and immune homeostasis. Nat. Rev. Immunol. 14, 141–153.
Pinton, P., et al., 2009. The food contaminant deoxynivalenol, decreases intestinal barrier permeability and reduces claudin expression. Toxicol. Appl. Pharm. 237, 41–48.
Preethi, J., et al., 2021. Facile synthesis of Zr(4+) incorporated chitosan/gelatin composite for the sequestration of Chromium(VI) and fluoride from water. Chemosphere 262, 128317.
Qazvini, N.T., Zinatloo, S., 2011. Synthesis and characterization of gelatin nanoparticles using CDI/NHS as a non-toxic cross-linking system. J. Mater. Sci. Mater. Med. 22, 63–69.
Rácz, R., et al., 2017. No change in bicarbonate transport but tight-junction formation is delayed by fluoride in a novel ameloblast model. Front. Physiol. 8, 940.
Rafique, T., et al., 2015. Geochemical controls of high fluoride groundwater in Umarkot Sub-District, Thar Desert, Pakistan. Sci. Total Environ. 530–531, 271–278.
Rahner, C., et al., 2001. Heterogeneity in expression and subcellular localization of claudins 2, 3, 4, and 5 in the rat liver, pancreas, and gut. Gastroenterology 120, 411–422.
Rao, J.N., et al., 2003. Polyamines regulate Rho-kinase and myosin phosphorylation during intestinal epithelial restitution. Am. J. Physiol. Cell Physiol. 284, C848–C859.
Schneeberger, E.E., Lynch, R.D., 2004. The tight junction: a multifunctional complex. Am. J. Physiol. Cell Physiol. 286, C1213–C1228.
Schwarz, B.T., et al., 2007. LIGHT signals directly to intestinal epithelia to cause barrier dysfunction via cytoskeletal and endocytic mechanisms. Gastroenterology 132, 2383–2394.
Shen, Q., et al., 2010. Myosin light chain kinase in microvascular endothelial barrier function. Cardiovasc Res. 87, 272–280.
Su, L., et al., 2013. TNFR2 activates MLCK-dependent tight junction dysregulation to cause apoptosis-mediated barrier loss and experimental colitis. Gastroenterology 145, 407–415.
Sun, H., et al., 2008. The Caco-2 cell monolayer: usefulness and limitations. Expert Opin. Drug Metab. Toxicol. 4, 395–411.
Sun, N., et al., 2020. Probiotic Lactobacillus johnsonii BS15 prevents memory dysfunction induced by chronic high-fluorine intake through modulating intestinal environment and improving gut development. Probiotics Antimicrob. Proteins 12, 1420–1438.
Takeichi, M., 2014. Dynamic contacts: rearranging adherens junctions to drive epithelial remodelling. Nat. Rev. Mol. Cell Biol. 15, 397–410.
Wang, H., et al., 2018. OTA induces intestinal epithelial barrier dysfunction and tight junction disruption in IPEC-J2 cells through ROS/Ca(2+)-mediated MLCK activation. Environ. Pollut. 242, 106–112.
Wang, H.W., et al., 2020. Fluoride-induced rectal barrier damage and microflora disorder in mice. Environ. Sci. Pollut. Res. Int 27, 7596–7607.
Wang, P., et al., 2001. Mechanisms of sodium fluoride-induced endothelial cell barrier dysfunction: role of MLC phosphorylation. Am. J. Physiol. Lung Cell Mol. Physiol. 281, L1472–L1483.
Wu, J., et al., 2020. Lanthanum chloride causes blood-brain barrier disruption through intracellular calcium-mediated RhoA/Rho kinase signaling and myosin light chain kinase. Metallomics 12, 2075–2083.
Wu, Y., et al., 2016. Protective effects of Lactobacillus plantarum on epithelial barrier disruption caused by enterotoxigenic Escherichia coli in intestinal porcine epithelial cells. Vet. Immunol. Immunopathol. 172, 55–63.
Xin, J., et al., 2021a. Preventive effects of Lactobacillus johnsonii on the renal injury of mice induced by high fluoride exposure: insights from colonic microbiota and co-occurrence network analysis. Ecotoxicol. Environ. Saf. 228, 113006.
Xin, J., et al., 2021b. Probiotic alleviate fluoride-induced memory impairment by reconstructing gut microbiota in mice. Ecotoxicol. Environ. Saf. 215, 112108.
Xu, H., et al., 2007. Effects of fluoride on the intracellular free Ca2+ and Ca2+-ATPase of kidney. Biol. Trace Elem. Res. 116, 279–288.
Xu, Z., et al., 2013. Relationship between intracellular Ca^{2+} and ROS during fluoride-induced injury in SH-SY5Y cells. Environ. Toxicol. 28, 307–312.
Yang, E., et al., 2010. Fluoride induces vascular contraction through activation of RhoA/Rho kinase pathway in isolated rat aortas. Environ. Toxicol. Pharm. 29, 290–296.
Zahs, A., et al., 2012. Inhibition of long myosin light-chain kinase activation alleviates intestinal damage after binge ethanol exposure and burn injury. Am. J. Physiol. Gastrointest. Liver Physiol. 303, G705–G712.
Zhang, K., et al., 2013. TGF-β1 induces the dissolution of tight junctions in human renal proximal tubular cells: role of the RhoA/ROCK signaling pathway. Int. J. Mol. Med 32, 464–468.
Zhang, W., et al., 2020. Changes in intestinal barrier functions and gut microbiota in rats exposed to zearalenone. Ecotoxicol. Environ. Saf. 204, 111072.
Zhang, X.Y., et al., 2021. Sishen pill maintained colonic mucosal barrier integrity to treat ulcerative colitis via Rho/ROCK signaling pathway. Evid. Based Complement Altern. Med 2021, 5536679.
Zhang, Y., et al., 2016. Fluoride induced endoplasmic reticulum stress and calcium overload in ameloblasts. Arch. Oral. Biol. 69, 95–101.
Zhao, G.P., et al., 2021. Imidacloprid increases intestinal permeability by disrupting tight junctions. Ecotoxicol. Environ. Saf. 222, 112476.
Zihni, C., et al., 2016. Tight junctions: from simple barriers to multifunctional molecular gates. Nat. Rev. Mol. Cell Biol. 17, 564–580.
Zinatloo, S., Qazvini, N.T., 2014. Inverse miniemulsion method for synthesis of gelatin nanoparticles in presence of CDI/NHS as a non-toxic cross-linking system. JNS 267–275.
Zinatloo, S., Qazvini, N.T., 2015. Effect of some synthetic parameters on size and polydispersity index of gelatin nanoparticles cross-linked by CDI/NHS system. JNS 137–144.
Zinatloo, Z., Zinatloo, S., 2019. Preparation and characterization of curcumin niosomal nanoparticles via a simple and eco-friendly route. J. Nanostruct. 9, 784–790.
Zou, Y., et al., 2018. Inhibition of Rho kinase protects against colitis in mice by attenuating intestinal epithelial barrier dysfunction via MLC and the NF-κB pathway. Int. J. Mol. Med. 41, 430–438.
Zuo, H., et al., 2018. Toxic effects of fluoride on organisms. Life Sci. 198, 18–24.